Pileup Reconstruction

Benda Xu
RCNS, Tohoku University
(Dated: 2013-07-25)

In this KamLAND internal note(KIN2013c), an algorithm of pileup reconstruction is described.
In order to check its validity and efficiency, the algorithm is applied to KamLAND ^{85}Kr minor decay branch coincidence in reactor phase.
The result of ^{85}Kr concentration in solar phase is $47.01\mu Bq/m^3 \pm 31.82\%$.

I. INTRODUCTION

The frontend electronics of DAQ system of KamLAND, FBE, acquires waveforms of PMTs within a time window of approximately 500ns when triggered (need reference!), with each waveform of 200ns. This is defined as a *FBE event*. The system is designed to cover one *physics event* in such a time window, which is mostly the case.

However, there is a small possibility that two physics events, either related intrinsically or by accident, occurs in one FBE event. Such FBE event is called *pileup-event* or *pileup* for simplicity. Present event reconstruction algorithm in KamLAND does not consider this case. It could give junk reconstruction results on pileups. To prevent these junk results polluting further analysis, a goodness-of-fit index based on likelihood[1, p. 143] is deployed, and called *badness* in RCNS[2, p. 120]. All events exceeding a certain badness are cut out.

The importance of pileup study lies in two cases.

If the two physics events in a pileup are related intrinsicly, e.g., successive decays of an isotope, we can tag such decays precisely by analysis. We have an application of this case: In solar phase of KamLAND, ^{85}Kr is one of the main backgrounds to our target signal, ^{7}Be ν[2, p. 171][1, p. 144]. ^{85}Kr has a minor decaying mode of branching ratio 0.434% which have a β decay followed by a γ with a immediate state half life of 1.015μs[3].

$$^{85}\mathrm{Kr} \xrightarrow[0.434\%]{\beta(173keV)} (9/2^+)^{85}\mathrm{Rb} \xrightarrow[\tau=1.015\mu s]{\gamma(5.14keV),100\%} (5/2^-)^{85}\mathrm{Rb}$$

By recontructing such events, we can get the concentration level of ^{85}Kr in KamLAND, as well as its time and spacial distribution.

If the two physics events in a pileup associated accidentally. It is more likely to happen at low energy where the event rate is high. The badness cut is not clean. Until now we do not have an estimation of type-I or type-II error. Therefore it is hard to estimate how many pileups remain and how it affects energy spectrum observed by KamLAND. The best example is the high energy tail of ^{210}Po peak[2, p. 165]: If we can tag pileup events, we can infer how many excess events of high energy tail of ^{210}Po come from ^{14}C-^{210}Po pileup. Chris did a simulation assuming rate of ^{14}C to modal the spectrum distortion effect of pileup[1, p. 130].

In this work, we confront pileups directly and develop an algorithm to reconstruct them for KamLAND.

II. ALGORITHM

To reconstruct pileups, we devide the process into the following stages:

1. Apply vertex fit algorithm for normal KamLAND events.
2. Identify pileups.
3. Selected FBE event is run though 1 dimensional K-means clustering algorithm for a best split.
4. Either piece of the split is passed to Kat[4] vertex and energy fitter.

A. Preliminary Vertex Fit

To prepare timing distribution of photo-electron (pe) for the following steps, a vertex fit is first applied. KamLAND has a detection volume of up to 6.5m radius sphere, applying vertex fit first to get time-of-flight (TOF) corrected pe timing distribution can narrow down the peaks.

In KamLAND offline analysis repository, vertex data are stored in *general vector file* (gvf). We use these v2 data directly for TOF corrected timing distribution(TCTD). If, however, gvf records a failure for an event, which is often the case for pileups, we apply *Kat vertex fitter* instead. That fitter tries to minimize the spread of the biggest peak in TCTD: It still helps even if not converge.

B. Identify Pileup

Pileup is rare, we need a fast and efficient method to identify pileup candidates. The special property to look for is multimodity of timing distribution of pe in each FBE event (Fig. 1(b)), as opposed to unimodity of normal events(Fig. 1(a)). *Modal* of a distribution can be viewed as peak of its probability distribution function(PDF).

Algorithms exist in literature to test unimodity, such as bandwidth of *kernel density estimation* [5], *dip test* [6] and *excess mass estimation* [7]. Here we select dip

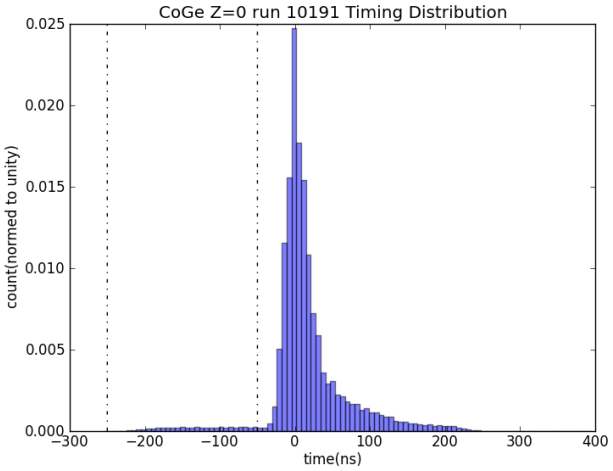

(a) normal event, unimodal

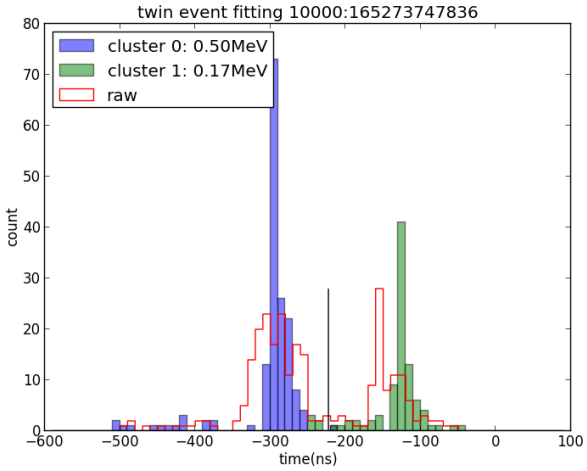

(b) pileup event, multimodal, vertical black line indicates a split

FIG. 1. examples of different types of events in KamLAND

test, as it has a well defined p-value (as opposed to kernel density estimation) and a well tested programming library available in R [8] (as opposed to kernel density estimation and excess mass estimation).

Dip algorithm tries to infer position and significance of the modal in a sample, assuming to be drawn from a unimodal distribution. The null hypothesis of dip test is that the sample is drawn from a uniform distribution, which represents the category of unimodal distributions. The alternative hypothesis of dip test is that the sample is drawn from a multimodal distribution of at least two modals. [6]

As depicted in Fig. 2, according to distribution of p-value of dip test, the event with p-value < 0.15 are selected for further process.

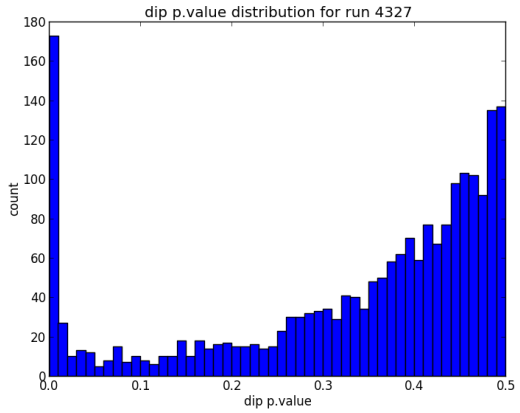

FIG. 2. distribution of [0, 0.5] subset of p value of dip test for delayed and prescaled events in reactor phase

C. Split Two Physics Events

As in Fig. 1(b), as long as an event is selected by previous step, it needs to be further splitted. This is the problem of *clustering* in machine learning with many well established algorithms.

Many of the algorithms, however, are opimized for high dimensions. For 1-dimension problem like what we have, further information can be extracted to aid the separation. Without a comprehensive survey of the subject, we select *K-means Clustering in One-dimension* algorithm, as it is available in R [9] and tested to work.

In this algorithm, the solution is a split S to produce clusters c_1 and c_2 s.t. withinss (within sum of squares) from each element to its corresponding cluster centre is minimized (Fig. 1(b)).

D. Physics Event Reconstruction

Once the TCTD is splitted into two clusters in previous step, time and charge of pe's involved in either cluster are retrived and normal event reconstruction algorithm is applied.

We have two sets of event reconstruction routines in KamLAND, Kat vertex/energy and v2/a2. The latter is a likelihood based fitter, which depends on light curves inferred from calibrations, and is therefore sensitive to the split in previous step. If the overlaps are not well handled, v2/a2 gets confused easily.

Therefore, we use Kat vertex/energy routine for robustness with a price of lower vertex and energy resolutions.

One attention needs to be paid. Although time window of a FBE event is 500ns, waveform length of each FBE channel is 200ns. That means if the first of the two

phyics events (prompt event) occupies one FBE channel, the second (delayed event) is either rejected (when time gap exceeds 200ns) or affected (time gap within 200ns) in that channel. That is, the channels occupied by the prompt event is effectively bad for delayed one. Therefore when reconstructing delayed events, we mask the channels occupied by the prompt with the same routine for bad channel handling with KChStatus class of Kat.

Candidate events which failed in fitting are thrown away.

III. PERFORMANCE CHECK

The check of performance, we could make a simulation of pileups and see how it is processed by the proposed algorithm. Such simulation is hard. At the time of writing we refering to two simple checks, one being ^{85}Kr concentration in reactor phase in the following section, the other being ^{203}Hg pileup[10].

IV. KRYPTON TAGGING IN REACTOR PHASE

As mentioned in Section I, ^{85}Kr has a minor branch of ratio 0.434% which gives pileups and can be tagged[3]. ^{85}Kr in KamLAND reactor phase is high in concentration [11, p. 165], therefore we first apply the algorithm here.

A. Data Set

In reactor phase, prompt trigger threshold is 200 or 180, which is too high in energy (99% efficiency at 0.88 MeV for γ [12, p. 32]). Delayed and prescaled thresholds are 120, which covers the energy window we want (99% at 570 keV for γ[12, p. 33]), and are after all the only usable event types with energy low enough. Readers are referred to trigger design of DAQ system in KamLAND ([13, p. 66]) to grasp the above argument.

The trigger thresholds are changed by KamLAND activities e.g. an electronic upgrade. According to the time variation of trigger conditions (Fig. 3), we select Runs 3575–6822 for this study.

B. Concentration

The average concentration of ^{85}Kr from Apr. 2004 to May 2007, is given by energy spectral fit of its major β decay. From Ref [11, p. 165], we have

$$N = N_0 2^{-\frac{\Delta T}{\tau}},$$

where τ is half life of ^{85}Kr, 10.76 years or 129.1 months. ΔT is months from May 2001, initial LS filling of KamLAND. N_0 is ^{85}Kr activity at initial filling, fitted by Hiroko as 381.3 ± 7.87 in R<5m[14]. Therefore the average

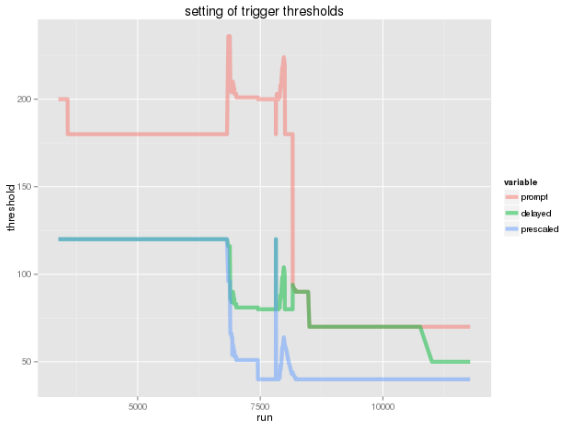

FIG. 3. time variation of trigger threshold

^{85}Kr concentration is estimated to be

$$\frac{N_0}{38}\sum_{\Delta T=35}^{72} 2^{-\frac{\Delta T}{\tau}} = 286.6Bq,$$

which is 547.4 mBq/m^3. We assign a uncertainty of 3% to account for uncertainty of N_0, τ, branching ratio of major β and month rounding of ΔT.

C. Event Selection and Efficiency

To apply various cut to data and filter out irrelavent events are referred as event selection. Serveral criteria are applied.

The number of events remaining is 30846 (Fig. 4).

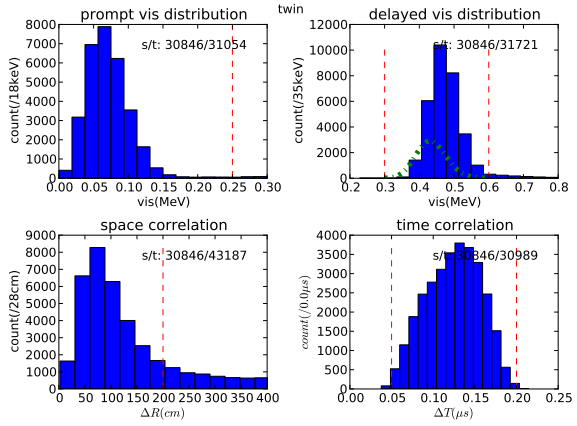

FIG. 4. plot of delayed coincidence events

1. *Deadtime and μ Veto*

As a common practice in KamLAND[11, p. 119], only runs evaluated to be *good* are used. Here we also select

runs longer than 1 hour. *Missing* μ and *trigger disabled period* are identified, and any following events within 2s are rejected[12, p. 132], using KamLAND *livetime* toolset available in RCNS. μ event together with any following events within 2ms are rejected.

Two approaches exist to calculate *livetime* (length of time the detector is sensitive to signal). We use the method of counting *1pps* trigger and are aware that the uncertainty is negligible.[12, p. 132] The livetime is counted to be 73312050s (about 848.5days or 2.32 years). Comparing with 1137 days spanning runs 3575-6822, it gives a ratio of 74.6%.

The number of expected events is therefore 5.4×10^6.

2. Trigger fraction

Delayed trigger is issued in a 1ms time window following a *prompt trigger* whose rate is 31.24 ± 0.02Hz(Fig. 5).

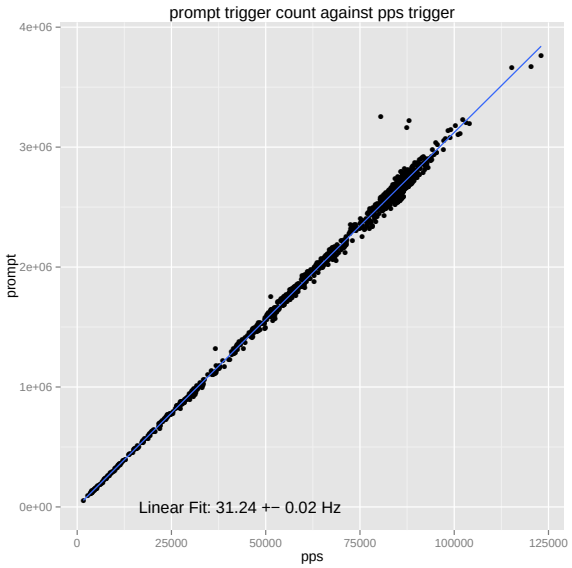

FIG. 5. Frequency of prompt trigger, time is counted as 1pps trigger.

Poisson process is used to model overlap between delayed time windows, the expected raw time window

$$\tau = \int_0^{t_0} \lambda t e^{-\lambda t} dt + t_0 \int_{t_0}^{\infty} \lambda e^{-\lambda t} dt,$$

where $\lambda = 31.24 \pm 0.02 Hz, t_0 = 1ms$. We have $\tau = 0.98454 \pm 0.00001 ms$. The time fraction of delayed trigger is then 0.03075 ± 0.00002.

An alternative can be made by counting prompt trigger, 2290584486, and substracting overlap of delayed window, 6634s, giving a time fraction of 0.03115.

The fraction of prescaled trigger is 0.01024, giving a total live time fraction by inclusion-exclusion principle to be 0.01024 + 0.03115 - 0.01024 × 0.03115 = 0.04107.

Note that the discontinuities of livetime cased by Sec IV C 1 is assumed to cancel each other. We assign a uncertainty of 2% here.

3. Hit Range

Hit (more precisely *Nhit17*) is defined as number of 17inch PMT (therefore usually corresponding FBE channel) with output signal exceeding that of one third of a pe. It serves as a rough energy estimator and we restrict our attention to events whose hits are less than 400 (˜2MeV in γ).

Using only events with delayed and prescaled trigger infers the ones with hit more than 120 are used.

We, however, can not make a precise estimation of how much percent of candidates falls below hit of 120. The energy scale and the miss ratio of fitter below 0.2MeV are not studied. Therefore, selection efficiency of hit range is covered in Section IV C 5, combined with those two unknown factors.

An investigation on Nhit17 distribution of selected events in Section IV C 6 indicates that a hit range of (120, 400) does not have false rejections practically. (Fig. 6)

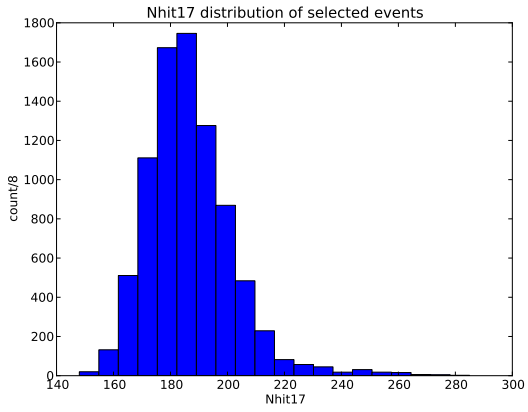

FIG. 6. Nhit17 distribution of selected events

4. Dip Test and split

In the dip test of the algorithm, only events with p-value < 0.15 are retained (Section II). The correctness of split is also included here. The efficiency, ϵ_{dip}, is a quantity we are going to estimate here. The efficiency of ΔT (Section IV C 6), depending on timing of DAQ system and fitter, is hard to estimate. So we include that into ϵ_{dip} as well. A cross check of ϵ_{dip} from ^{203}Hg calibration is available[10], which shows that ϵ_{dip} fails within 70%˜100%.

5. Fit and Prompt Energy Efficiency

In step 3,4 of the algorithm, events that failed in fitting are thrown away. Further more, event pair in which prompt event fitted to be after delayed event indicates failure in fitting (Fig. 7), and is rejected.

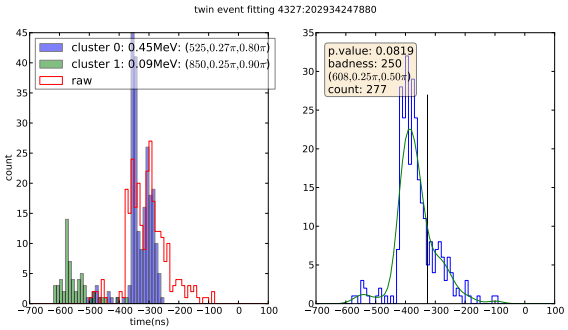

FIG. 7. Left: failed fit, could be identified as the second(green) cluster fitted before the first(blue). Right: wrong splitting causing the failure.

The energy scale and the miss ratio of fitter below 0.2MeV are unknown.

The efficiency covering all these factors, $\epsilon_{\rm fit}$, is also a quantity we are going to estimate here. A cross check of $\epsilon_{\rm fit}$ from cross-event delayed coincidence is available[15], which shows that $\epsilon_{\rm fit}$ fails within 2%~10%.

6. Delayed Conincidence and Background

In order to get target ^{85}Kr decays, a set of selection rules called *delayed conincidence* are applied to the physics event pairs reconstructed.

- $E_p < 250$KeV (in visible energy)
- 300keV $< E_d <$ 600 keV
- $\Delta R <$ 2m
- R_p, $R_d <$ 5m
- 50ns $< \Delta T <$ 200ns

As E_p is covered by $\epsilon_{\rm fit}$, E_d is essentially 100%, ΔT is covered by $\epsilon_{\rm dip}$, the factor left for us to play with is ΔR.

Accidental coincidence is one of the backgrounds, either of the component event is assumed to distribute uniformly within R<5m. Here we use ΔR and D interchangably, and derive PDF h(D) as

$$h(D) = \int g(D, r_0) f(r_0) dr_0,$$

where $f(r_0)$ is PDF of the first event, uniform within fiducial volume(FV), $g(D, r_0)$ is the joint PDF.

$g(D, r_0)$ can be calculated like this. In Fig. 8(a), $\odot O$ is FV of R<5m. P is the first event ($r_0 := OP$). The second is on $\odot P$ of redius D. $\odot O$ and $\odot P$ has intersections A and B, arc PAC gets counted. When $R > D + r_0$, $\odot P$ gets fully counted. In the first case,

$$g(D, r_0) \propto (R^2 + 2r_0 D - r_0^2 - D^2) r_0 D.$$

Accidental background is fitted in a region of $D > 6m$. ^{85}Kr is inferred from substraction(Fig. 8(b)), 29632 ± 20 after $\Delta R < 2m$ cut. We defer a vertex resolution model for ^{85}Kr as future improvement. Study of such model in calibration can be found in [11, p. 58].

Another background is from $^{212}Bi^{212}Po$ delayed coincidence[2, p. 156], which can only be rejected by E_d and partially by E_p cuts. We do not have a good estimation of contribution after the energy cuts because the scale is largely unknown. A calculation indicates that it is negligible[16]. We do not explicitly consider it, and the systematic uncertainly introduced is less than 1%.

It is worth mention that, the accidental background, mainly caused by $^{14}C^{210}Po$ pileup, contributes to the mysteries high energy tail of ^{210}Po. That is a major background in KamLAND solar phase[2][1].

7. Summary

The analysis can be viewed as passing events through a series of filters. The filtering power is summarized in Table I.

TABLE I. Selection Ratios

raw	3416077056	%
muon, deadtime, hit, trigger type	2007297696	58.760
dip	696572	0.035
sep and fit	633216	90.905
delayed coincidence	30846	4.871

We can only calculate the production of $\epsilon_{dip}, \epsilon_{fit}$. To do that, total efficiency is divided by all known efficiencies. We have $\epsilon_{dip}\epsilon_{fit} = 0.0980 \pm 3.61\%$ (Table II).

V. KRYPTON TAGGING IN SOLAR PHASE

In two purification campaigns, KamLAND has ^{85}Kr reduced by more than 5 order of magnitudes[17, p. 173]. In solar phase, ^{85}Kr is nearly undetectable and has a large uncertainty[2, p. 174][18]. We apply our method to solar phase.

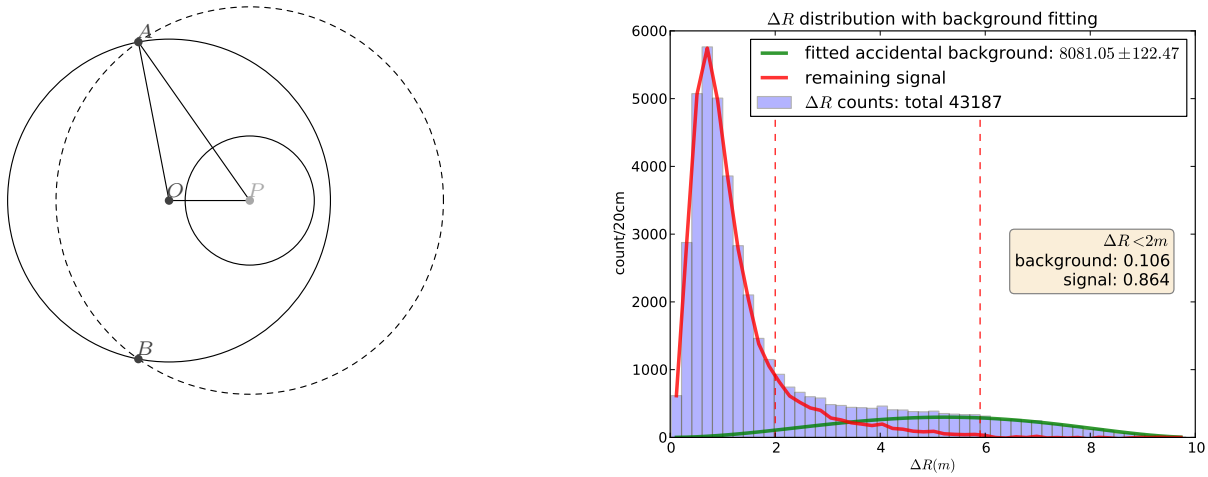

(a) Illustration of $g(D, r_0)$

(b) Fitting against ΔR

FIG. 8. Inferrence of background and signal on ΔR distribution

TABLE II. Calculation of ϵ_{dip} ϵ_{fit}

	value	relative uncertainty (%)
livetime(s)	73312050	0
Kr in R<5m(Bq)	286.6	3
branching ratio	0.00434	0
expected	91188754	3
observed	29632	0.067
total efficiency	3.249523e-04	3
delayed + prescaled	0.04107	2
ΔR	0.859	0
ΔT	0.094	0
$\epsilon_{dip}\epsilon_{fit}$	0.0980	3.61

A. Data Set

All runs that are longer than 1 hour and tagged *good* in KamLAND solar phase, 8502-10320, is used.

Livetime is counted with 1pps trigger to be 41025839s (about 474.84 days or 1.30 years). The runtime being 712 days, giving a livetime ratio of 66%.

B. Light Yield Change

Purification campaigns made attenuation length of liquid scintillator in KamLAND smaller and light yield (LY) lower. An estimation from Kyohei gives raw LY at the spot of event in LS decreases 15%[2, p. 81]. *detectable LY*, the remaining photon after collected by PMT, used with LY interchangably here, recognized by waveform analysis and event reconstruction, is way more lower.

An quantitative interpretation of energy resolution by detectable LY is given by Benda[19], which changes from 268.74MeV^{-1} ($\sigma/\sqrt{E}$ = 6.1%) to 204.08MeV^{-1} ($\sigma/\sqrt{E}$ = 7%). We use the detectable LY estimation of 25% decrease.

The most significant affect of LY decrease is the prompt events, which fail below 200keV and more than half is undetectable by KamLAND(Fig. 9). When LY decreases such efficiency gets worse. We made a rough estimation of this effect as given in Fig. 9: The β spectrum was calculated with energy scale model of KamLAND[2, p. 89], and scaled with an additional factor to fit the observed spectrum in reactor phase (Section IV) above 75keV. The efficiency curve is then inferred by division of the observed spectrum by the expected. Then for solar phase we further scale the expected spectrum by LY decrease, 25%, and multiply with the efficiency curve. The prompt efficiency is then estimated to descrease by 25%, from 0.449 to 0.336 (Fig. 9).

We keep in mind energy scale is mostly unknown at this energy region, and expect half of the change is uncertain. Then we get a reduction factor of 0.75 ± 0.13 in efficiency.

C. Event Selection

All the event selection methods in Section IV C are used, with several exceptions.

We use *single trigger* in solar phase, it is issued 100% of the livetime. Hit range is set to from 80, the single trigger threshold, to 300, an Nhit17 high enough after light yield decrease.

After all the selections, 43 events remains (Fig. 10). There seems to be a low energy cluster in E_{delayed} from

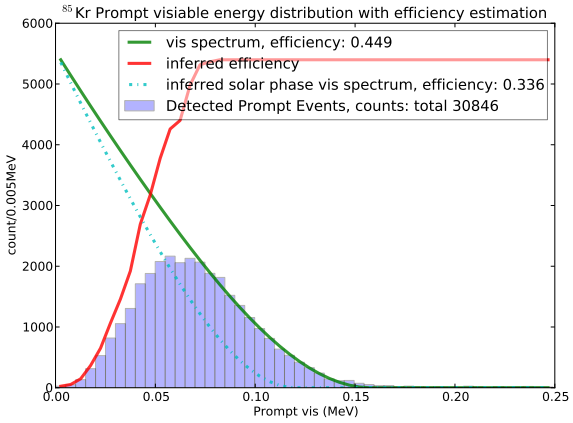

FIG. 9. Rough estimation of prompt event detection efficiency

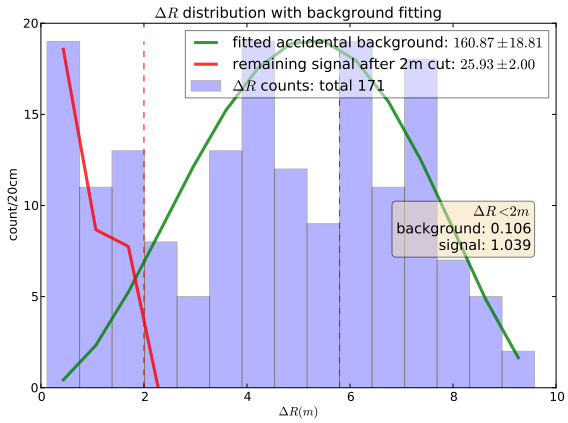

FIG. 11. ΔR plot to separate from background

accdidental coincidence. if we apply a stricter cut of 350keV, 25 events remains.

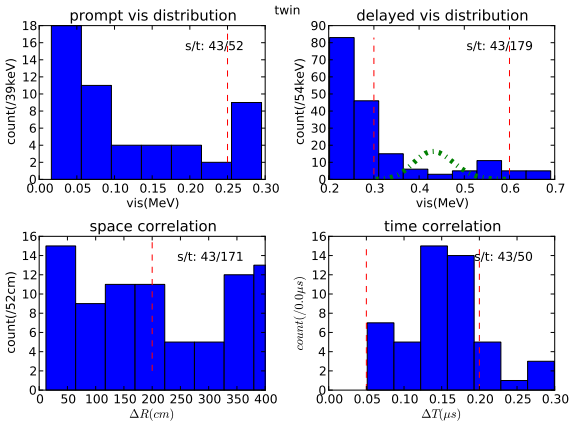

FIG. 10. delayed coincidence plot for solar phase

D. R Fit

The same accidental background curve is used as reactor phase(Section IV C 6).

The remaining signal candidate is then 25.93 ± 2.00 after background subtraction (Fig. 11). After accounting for uncertainty from poisson count of 43, the signal is 25.93 ± 6.86, relative uncertainty being 26.44% (Table IV).

E. Summary

As Table I, we make the corresponding one for solar phase in Table III.

Affect of vertex resolution of on efficiency of ΔR cut is ignored. Then the ^{85}Kr concentration level is calculated

TABLE III. Selection Ratios of Solar Phase

raw	5035432537	%
muon, deadtime, hit	4148948355	82.395
dip	3719871	0.090
sep and fit	2949734	79.297
delayed coincidence	40	0.001
$E_{delayed}$ 350keV	25	62.500

to be $47.01 \mu Bq/m^3 \pm 31.82\%$.

TABLE IV. ^{85}Kr concentration calculation

	value	relative uncertainty (%)
$\epsilon_{dip}\epsilon_{fit}$	0.0980	3.61
light yield decrease	0.75	17.33
ΔR	0.859	0
ΔT	0.094	0
efficiency	5.93e-03	17.70
observed	25.93	26.44
total minor decays	4372.68	31.82
branching ratio	0.00434	0
livetime(s)	41025839	0
Kr activity(Bq)	0.0246	31.82
Fiducial Volume(m^3)	523.3	0
Kr Concentration($\mu Bq/m^3$)	47.01	31.82

VI. CONCLUSION

We developed a pileup reconstruction program in order to get ^{85}Kr concentration in KamLAND solar phase. The

algorithm efficiency $\epsilon_{\rm dip}\epsilon_{\rm fit}$ is evaluated to be 0.0980 ± 3.61% by applying to reactor phase.

The same algorithm is applied to solar phase, and 25.93 ± 6.86 events candidates are observed. The ^{85}Kr concentration is then calculated to be $47.01\mu Bq/m^3$ ± 31.82%.

This is higher than previous works (Fig. 12)[2, p. 174][1, p. 147][20, p. 95][18]. Unknown background may be miscounted as signals, a further investigation will be needed for $^{212}Bi^{212}Po$. Unknown systematic uncertainties may exist, too.

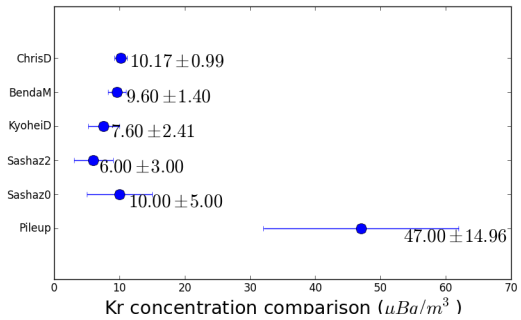

FIG. 12. Comparison of Kr concentration results

Several things could be done to improve the present result:

1. Cluster spliting algorithm is not perfect (Fig. 7). We can use several methods including the auxillary output from dip and peak finding in kernel density estimation, to cross check with the present Ckmeans in order to give better splittings.

2. As noted in ^{203}Hg pileup check[10], energy scale of $E_{\rm prompt}$ and $E_{\rm delayed}$ are largely uncertain due to dark charge. This issue can only be solved completely with a fitter reconstructing prompt and delayed events simultaneously.

3. Only good runs in solar phase are used, and the runtime coverage is only 66%, we could further make use of *half bad* runs to increase the statistics. Also, zen phase of KamLAND can be used to extend statistics.

4. When we have a better understanding on energy scale, maybe as a by-product of $^{14}C^{210}Po$, we could get further understanding of the unknown background seen in this study (Section V C).

5. Efficiency of this study is limited by ΔT. By deploying MoGURA electronics with *roll-back trigger* technology, we can boost the detection efficiency theoretically up to 10 times.

[1] C. P. Grant, *A Monte Carlo Approach to ^{7}Be Solar Neutrino Analysis with KamLAND*, Ph.D. thesis, University of Alabama (2011).

[2] K. Nakajima, *First Results from ^{7}Be Solar Neutrino Observation with KamLAND*, Ph.D. thesis, Tohoku University (2010).

[3] H. Sievers, Nuclear Data Sheets **62**, 271 (1991).

[4] KamLAND Analysis Toolkit.

[5] B. W. Silverman, Journal of the Royal Statistical Society. Series B (Methodological) **43**, pp. 97 (1981).

[6] J. Hartigan and P. Hartigan, Ann. Stat. **13**, 70 (1985).

[7] D. Muller and G. Sawitzki, J. Am. Stat. Assoc. **86**, 738 (1991).

[8] M. Maechler, "Hartigan's dip test statistic for unimodality," `http://cran.r-project.org/web/packages/diptest`.

[9] J. Song and H. Wang, "Optimal distance-based clustering for one-dimensional data," `http://cran.r-project.org/web/packages/Ckmeans.1d.dp`.

[10] B. Xu, "Pileup in ^{203}hg calibration," (2013), kamLAND Internal Note 2013b.

[11] H. Watanabe, *Comprehensive Study of Anti-neutrino Signals at KamLAND*, Ph.D. thesis, Tohoku University (2012).

[12] O. Tajima, *Measurement of Electron Anti-Neutrino Oscillation Parameters with a Large Volume Liquid Scintillator Detector, KamLAND*, Ph.D. thesis, Tohoku University (2003).

[13] E. Sanshiro, *Neutrino Geophysics and Observation of Geo-Neutrinos at KamLAND*, Ph.D. thesis, Tohoku University (2005).

[14] There is a typo in bottom part of [11] Figure 6.6, in which it should be R<5m instead of R<5.5m.

[15] K. Nakajima, "Delayed coincidence analysis of ^{85}kr (3)," `http://www.awa.tohoku.ac.jp/~kyohei/analysis/analysis_070820.pdf`.

[16] B. Xu, "An analysis of kr-85 at kamland," JPS Meeting at Hiroshima (2013).

[17] G. J. Keefer, *First Observation of ^{7}Be Solar Neutrinos with KamLAND*, Ph.D. thesis, University of Alabama (2009).

[18] A. Kozlov, "The kr-85 activity in kamland ls," (2011), kamLAND Collaboration Meeting at Alabama, `http://www.awa.tohoku.ac.jp/~kozlov/Kr_in_LS.pdf`.

[19] B. Xu, "Energy resolution model with gamma distribution," (2012), kamLAND Collaboration Meeting at Hawaii, `http://www.phys.hawaii.edu/~kamland/protected/CollabOct12/talks/EnergyRes-Benda_Hawaii.pdf`.

[20] B. Xu, *Observation of Be-7 Solar Neutrinos with KamLAND*, Master's thesis, Tohoku University (2011).